Scale Changing Technique for the Electromagnetic Modelling of MEMS-controlled Planar Phase-shifters

Étienne Perret, *Student Member, IEEE,* Hervé Aubert, *Senior Member, IEEE,* and Hervé Legay

***Abstract*— A scale changing approach is proposed for the electromagnetic modelling of phase-shifter elements used in reconfigurable MEMS-controlled reflectarrays. Based on the partition of the discontinuity plane in planar sub-domains with various scale levels this technique allows the computation of the phase shift from the simple cascade of networks, each network describing the electromagnetic coupling between two scale levels. The high flexibility of the approach associated with the advantages of the Integral Equations Formulations renders this original approach powerful and rapid. The scale changing technique allows computing quasi-instantaneously the *1024* phase-shifts achieved by *10* RF-MEMS switches distributed on the phase-shifter surface. Moreover the proposed approach is much better than the FEM-based software in time costing. Experimental data are given for validation purposes.**

***Index Terms*— multiscale structures, RF-MEMS, planar phase-shifter, reflectarrays.**

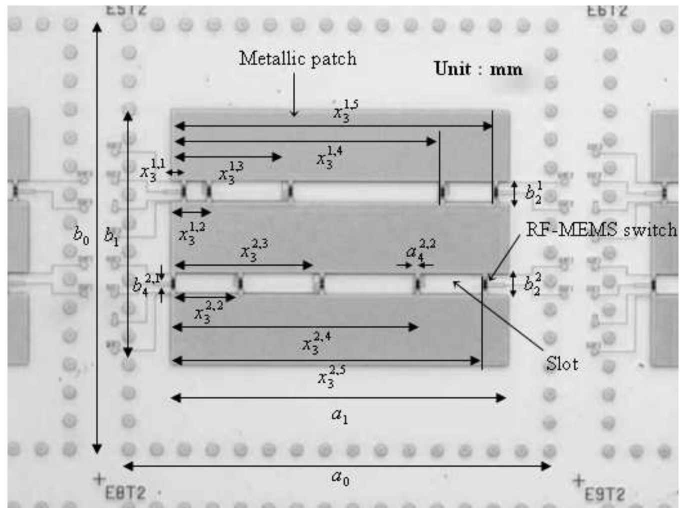

Fig. 1. Planar phase-shifter used in Ku-band MEMS-controlled reflectarrays. The structure has been manufactured on an alumina substrate (relative permittivity: *9.8*; thickness: *0.254 mm*). One side of the substrate is shown in this figure. The opposite side of the alumina substrate is completed by adding an air layer of thickness h = *2* mm followed by a metallic plane (short-circuit). For experimental purpose, this planar structure is inserted in the cross section of a metallic waveguide [12].

I. Introduction

Reflectarray consists of a feeding antenna illuminating a planar microstrip array which is designed to scatter a planar phase surface in front of the aperture [1,2]. The introduction of a specific small phase-shift for reconstituting a planar phase surface in the desired direction may be achieved by using microstrip patches with passive delay lines [3-5], by adjusting the patch size [6,7] or else, by tuning the substrate height [8]. Reflectarray antenna with Radio-Frequency Micro-Electromechanical Switches (RF-MEMS) is an emerging technology for reconfigurable and scanning antennas. A scanning antenna may be used for high-rate data transmission between nano-satellites flying in formation, beam steering for radar antenna and beam hopping for a multimedia antenna. The need for reconfigurable antenna is mainly related to flexibility. Such antenna allows the redefinition of their initial reserved missions. Moreover in-orbit sparse antennas are often required for global coverage systems, which would substitute any failing antenna. Recently circular [9] and linear [10] polarization reflectarrays controlled by RF-MEMS have been selected for two applications where MEMS technology offers interesting capabilities: (1) for Ka-band transmission of high flow between small satellites, observation and scientific expeditions of nano-satellites constellation and, (2) for Ku-band missions *GEO-telecom* requiring a reconfigurable satellite cover. In such reflectarray antenna the phase-shift variation is controlled by the UP/DOWN state of a finite number of RF-MEMS switches: for a phase-shifter element containing N switches, 2^N phase-shifts are available. In this paper we focus on the electromagnetic modelling of planar phase-shifters used in linear polarization reflectarrays controlled by RF-MEMS. In [10-12] the concept of MEMS-controlled reflectarray is developed and a strong need for an accurate and rapid electromagnetic simulation tool is clearly identified.

For optimization purposes fast and accurate electromagnetic simulations of a single phase-shifter element are needed. However classical full-wave methods –i.e., the Method of Moment or the Finite Element Method– require in this case a large computer storage capability and are very time-consuming as the number of switches increases. Moreover the wide diversity of scales –in practice the ratio between the largest and smallest dimensions in a single phase-shifter element is

E. PERRET is with the École Nationale supérieure d'Électrotechnique, d'Électronique, d'Informatique, d'Hydraulique et des Télécommunications, 2, rue Charles Camichel, 31071 Toulouse, France.

H. AUBERT is with the Laboratoire d'Analyse et d'Architecture des Systèmes, Centre National de la Recherche Scientifique, Toulouse, France, and with the École Nationale supérieure d'Électrotechnique, d'Électronique, d'Informatique, d'Hydraulique et des Télécommunications, France (corresponding author : H. AUBERT, phone : 33 5 61 58 84 50; e-mail: aubert@enseeiht.fr).

H. LEGAY is with the Space Antenna Departement, ALCATEL ALENIA SPACE, 26 Avenue JF Champollion, BP1187, 31037 Toulouse France.

higher than *100*– may generate ill-conditioned matrices in the numerical treatment of the boundary value problem. The Integral Equation Formulation (IEF) with entire domain trial functions [13] allows a reduction in the number of unknowns but suffers from low flexibility. An original approach, named *the scale changing technique*, is proposed here for handling the multiscale nature of the structure. Using a partition of the discontinuity plane in multiple planar sub-domains of various scale levels, the scale changing technique allows the computation of the phase-shift variation generated by the MEMS-controlled phase-shifter from the simple cascade of networks, each network describing the electromagnetic coupling between two scale levels. Very recently, this approach has been applied with success to the computation of the input impedance of planar antennas [14]. The application of the Scale Changing Technique to MEMS-controlled planar phase-shifters is more complex because it requires to handle many scale levels. A large collaborative research work has been reported in [10] including multiple industrial-oriented considerations relative to the design, the technology and the manufacturing of MEMS-controlled reflectarrays: this report is not focused on the numerical technique and does not give concrete numerical results for evaluating the key advantages (low computation time, high flexibility) of the Scale Changing Technique compared with classical numerical techniques. Finally, the research work reported in [15] is focused on the derivation of the equivalent network of a single RF-MEMS switch and is not concerned with the electromagnetic modelling of multi-scale planar circuits: in [15] the scale changing technique could be viewed as a special case of the Mode Matching Technique. In the present paper, on the one hand, multiple scale levels are taken into account by an original cascade of more than one scale changing networks and, on the other hand, present application is distinct from the authors' previous work.

The paper is organized as follows: in Section II the scale changing technique is applied to the electromagnetic modelling of a planar phase-shifter used in MEMS-controlled reflectarrays and key general characteristics of the proposed method are given. The computational results and experimental validations are presented in Section III. The *1024* phase-shifts obtained from a phase-shifter element with *10* RF-MEMS switches are calculated and discussed. Finally, the ratio between the DOWN- and UP-state capacitances providing a range of *360*° phase-shift is determined.

II. THE SCALE CHANGING TECHNIQUE

A. the MEMS-controlled planar phase-shifters

For the sake of clarity in the theoretical developments let us consider planar phase-shifters composed of *3* metallic patches and *10* RF-MEMS switches (see Fig. 1). Note that the approach can be applied to planar phase-shifter with arbitrary numbers of patches and RF-MEMS switches. Such phase-shifters have been advantageously used as the cells of reconfigurable MEMS-controlled reflectarrays [10-12]: the UP/DOWN states and positions of the switches allow several operating modes and interesting discrete tuning of the slit length. Experimental characterizations are generally carried out by placing the planar phase-shifter in the cross section

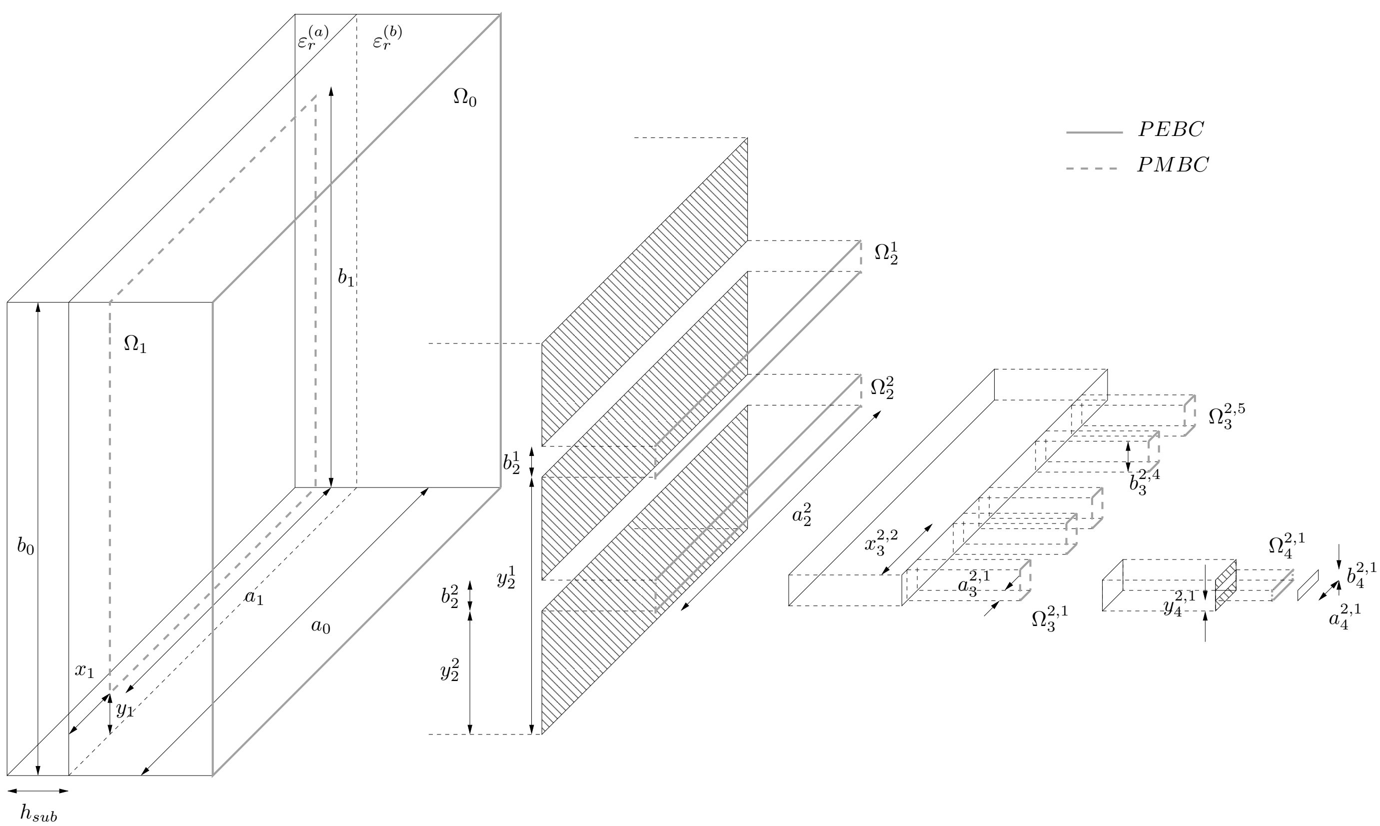

Fig. 2. A multi-scale view of the planar phase-shifter located in the cross section of a metallic waveguide.

of a metallic rectangular waveguide and by considering a TE_{10} incident mode [12]. In this Section, the scale changing technique is applied for predicting the phase-shift introduced by the phase-shifter on the TE_{10}-mode. Computational results are compared with measurements in the next Section. As illustrated in Fig. 2, at each scale level $s_l = [0:4]$, planar regions or domains may be defined as follows:

- at scale level $s_l = 0$, the waveguide cross-section defines the rectangular domain Ω_0;
- at scale level $s_l = 1$, the rectangular domain Ω_1 of surface S_1 gathers together the three patches, the two slit and the *10* RF-MEMS switches;
- at scale level $s_l = 2$, the slot domain Ω_2^i(with $i = [1, 2]$) of surface S_2^i ($< S_1$) is particularized;
- at scale level $s_l = 3$, the domain $\Omega_3^{i,j}$ of RF-MEMS switches (with $i = [1, 2]$ and $j = [1 : 10]$) of surface $S_3^{i,j}$ ($< S_2^i$) is identified;
- finally, at the smallest scale level $s_l = 4$, the movable part $\Omega_4^{i,j}$ of the RF-MEMS switch is defined.

As indicated in Fig. 2, the domain Ω_1 is bounded by perfect magnetic conditions while Ω_2^i, $\Omega_3^{i,j}$ and $\Omega_4^{i,j}$ are enclosed by perfect magnetic and electric conditions. These boundary conditions are imposed at the contour of the various domains and are assumed to not greatly perturb the electromagnetic field in the structure. Due to the formulation of such (artificial) boundary conditions, the scale changing technique is an approximate approach and not an exact method. Note that the natural basis for expanding the current density on the domain Ω_1 (i.e., on the metallic patch) is the set of modes in a rectangular waveguide of cross section Ω_1 and bounded by *magnetic* walls. However, as far as the numerical convergence is reached, we have observed numerically that the set of modes in a rectangular waveguide of cross section Ω_1 and bounded by *electric* walls provides to reach also an accurate solution for the phase-shift, but with an high number of modes. Consequently the choice between magnetic and electric boundary conditions seems to be not critical. The electromagnetic field in each domain Ω (with $\Omega = \Omega_1$, Ω_2^i, $\Omega_3^{i,j}$ and $\Omega_4^{i,j}$) can be expanded on the set of propagating and evanescent modes in an artificial waveguide of cross section Ω. As reported in the Section II.B, from such field representation, scale changing networks can then be derived for the modelling of the electromagnetic coupling between two successive scale levels s_l and $s_l + 1$.

B. Scale changing network

The network representation of the electromagnetic coupling between two successive scale levels is now derived.

As sketched in Fig. 3 (a) consider the domain Ω_{s_l} at scale level s_l as a discontinuity plane Ω_{s_l} composed of the sub-domain Ω_{s_l+1} (at scale level $s_l + 1$) and the complementary perfect electric or magnetic domain $\bar{\Omega}_{s_l+1}$. By adopting the set of propagating and evanescent modes in the two artificial waveguides of cross sections Ω_{s_l} and Ω_{s_l+1}, the impedance or admittance matrix of the discontinuity plane can be derived from a Multimodal Variational Technique [16]. High order evanescent modes are shorted by their (pure imaginary) impedance and are said *passive* and, propagating and low order evanescent modes –or *active* modes– are used to model the electromagnetic coupling between two successive scale levels. The number of active and passive modes is determined a posteriori from the numerical convergence of the phase-shift. Active modes are symbolized by ports in the network representation of the discontinuity plane given in Fig. 3 (b). This network, called here the *scale changing network*, is then characterized by its impedance $[Z_{s_l,s_l+1}]$ or admittance $[Y_{s_l,s_l+1}]$ matrix such that:

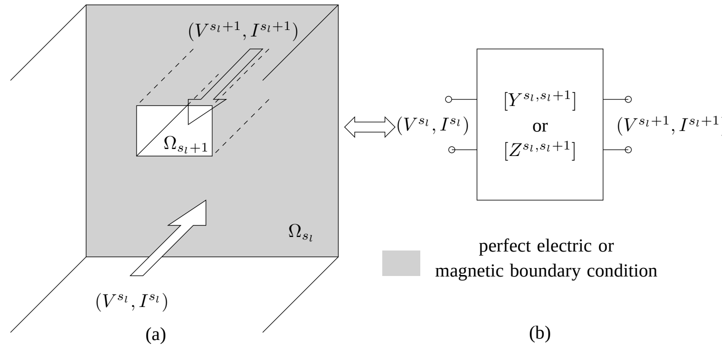

Fig. 3. (a) Discontinuity plane considered as a building block in the scale changing technique, and (b) its equivalent network, called here the *scale changing network*.

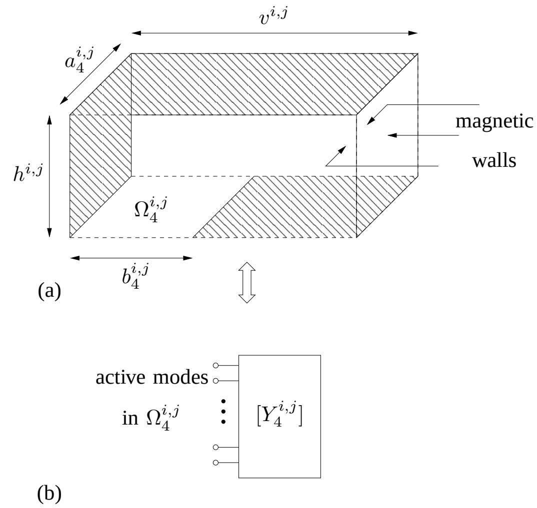

Fig. 4. (a) RF-MEMS switch used in the phase-shifter at the smallest scale, and (b) its equivalent network.

$$\begin{bmatrix} V_{s_l} \\ V_{s_l+1} \end{bmatrix} = [Z_{s_l,s_l+1}] \begin{bmatrix} I_{s_l} \\ I_{s_l+1} \end{bmatrix}$$
$$or \tag{1}$$
$$\begin{bmatrix} I_{s_l} \\ I_{s_l+1} \end{bmatrix} = [Y_{s_l,s_l+1}] \begin{bmatrix} V_{s_l} \\ V_{s_l+1} \end{bmatrix}$$

where (V_s, I_s) denote respectively the voltage and current magnitudes of active modes at scale level s ($s = [s_l, s_l + 1]$).

C. Surface impedance matrix for RF-MEMS switches

Fig. 4 (a) displays the geometry of RF-MEMS switch in the domain $\Omega_4^{i,j}$ ($i = [1, 2]$ and $j = [1 : 10]$). As reported in [15], the set of propagating and evanescent modes in an

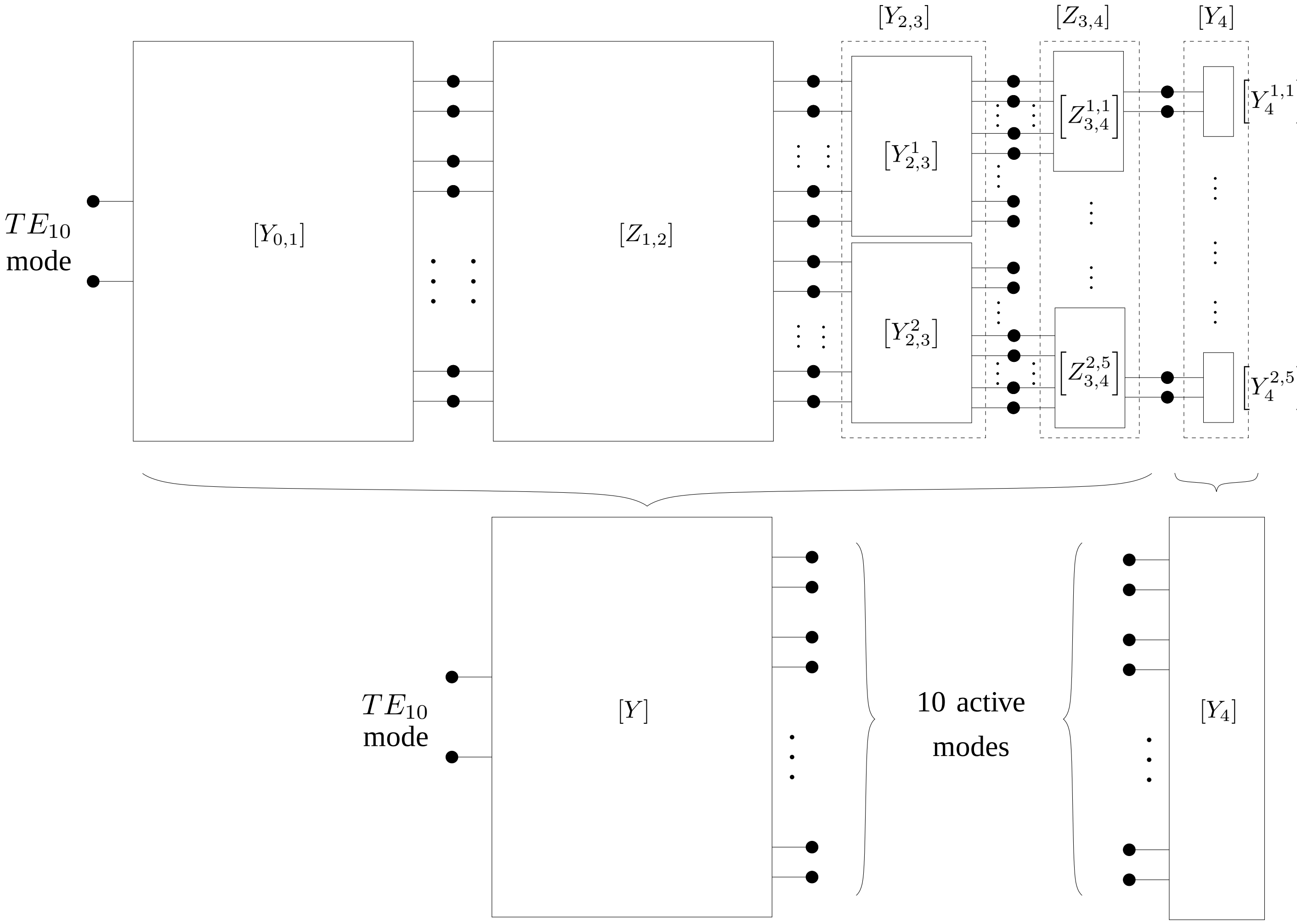

Fig. 5. Equivalent network of the phase-shifter as the cascade of scale changing networks shunted by the equivalent networks of the RF-MEMS switches.

artificial waveguide of cross section $\Omega_4^{i,j}$ allows the derivation of the multi-port network modelling the RF-MEMS switch. Note that, if only one active mode –i.e., the TEM mode– is adopted in the domain $\Omega_4^{i,j}$, the network is equivalent to the surface impedance $Z_s = \frac{1}{jC_{MEMS}^{i,j}\omega}$, where the capacitance $C_{MEMS}^{i,j}$ is given by

$$C_{MEMS}^{i,j} = 2\varepsilon_o \frac{b_4^{i,j} h^{i,j}}{v^{i,j}} \sum_{n=0,1,2,\ldots}^{+\infty} \frac{\coth\left(\gamma_{2n+1}^{i,j} h^{i,j}\right)}{\gamma_{2n+1}^{i,j} h^{i,j}} \ldots \left\{ \frac{\sin\left[(2n+1)\frac{\pi}{2}\frac{b_4^{i,j}}{v^{i,j}}\right]}{(2n+1)\frac{\pi}{2}\frac{b_4^{i,j}}{v^{i,j}}} \right\}^2 \quad (2)$$

with

$$\left(\gamma_{2n+1}^{i,j}\right)^2 = \left[(2n+1)\frac{\pi}{2v^{i,j}}\right]^2 - k_0^2$$

and k_0 designates the free-space wavenumber.

D. Formulation of the scale changing technique

As shown in Fig. 5 the equivalent network of the MEMS-controlled planar phase-shifter is obtained from the cascade of *4* scale changing networks. Each networks model the electromagnetic coupling between two successive scale levels. The cascade is shunted by *10* multi-port networks, each modelling a RF-MEMS switch. Following Sections II.B and II.C, all the networks are computed separately. The analytical expressions of their impedance or admittance matrices are reported in Appendix. The input impedance Z_{in} of the cascade is then computed and the phase ϕ of the reflection coefficient is finally deduced from the following relationship

$$\phi = Arg\left[\frac{Z_{in} - Z^{TE_{10}}}{Z_{in} + Z^{TE_{10}}}\right] \quad (3)$$

where $Z^{TE_{10}}$ designates the impedance of the TE_{10}-mode. The number of active modes in all impedance or admittance matrices is such that the numerical convergence of the phase ϕ is reached.

Before presenting the computational results and experimental validations, let us point out key characteristics of the proposed scale changing technique. As introduced in Section II.A this technique is based on the partition of the discontinuity plane in multiple domains of surface S_{s_l} (with $S_1 > S_2 > \ldots$). In order to eliminate numerical problems due to the treatment of ill-conditioned matrices, the partition

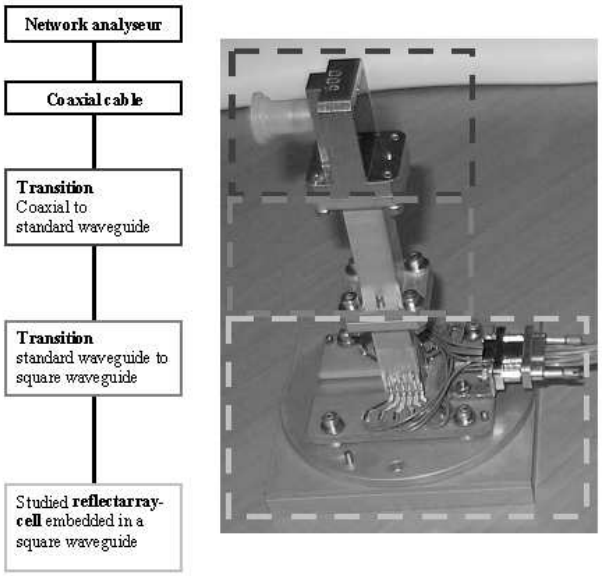

Fig. 6. Measurement cell [10,11].

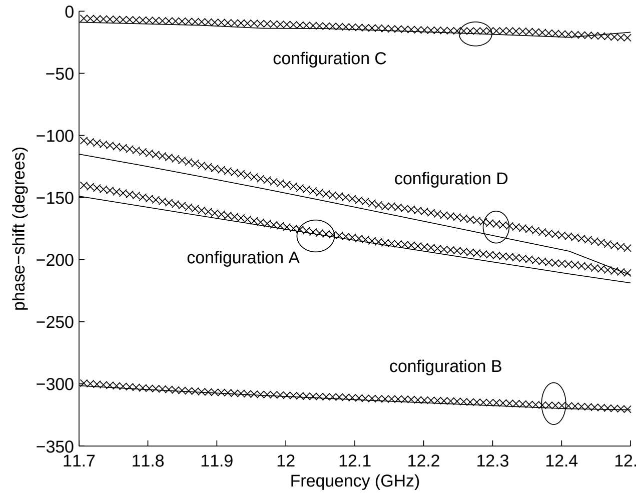

Fig. 7. Phase-shift versus frequency for 4 various UP/DOWN state configurations of the 10 RF-MEMS switches: configuration A: [00000 00000]; configuration B: [11111 00000]; configuration C: [11011 11111]; configuration D: [11001 00000]; where the first *5* digits designate the UP/DOWN states of switches in one slot Ω_2^2 (the digit is *0* when the state in DOWN) and the last *5* digits describe the states of the switches in the other slot Ω_2^1. (—) Measurements; ($\times\times\times$) Scale Changing Technique. Dimensions are (see Fig. 1, unit : mm): a_0=15, b_0=15, a_1=12, b_1=9, b_2^1=b_2^2=0.75, $a_4^{2,2}$=0.1, $b_4^{2,1}$=0.1, $x_3^{1,2}$=2.4, $x_3^{1,3}$=5.3, $x_3^{1,4}$=8.7, $x_3^{1,5}$=11.1, $x_3^{2,1}$=0.45, $x_3^{2,2}$=1.35, $x_3^{2,3}$=4.25, $x_3^{2,4}$=9.65 and $x_3^{2,5}$=11.15.

can be chosen in order to avoid critical aspect ratios: two successive scale levels s_l and s_l+1 may be such that, for instance, $S_{s_l}/S_{s_l+1} < 100$. Moreover, at each scale level s_l, the electromagnetic field can be described as precisely as wished by taking an appropriate number of modes in the corresponding domain. Finally, since the computation of all the networks can be performed separately, a modification of the phase-shifter geometry at scale s_l requires the recalculation of only two scale changing networks. In other words the partition of the discontinuity plane in multiple domains makes the approach modular (Lego approach). Note that the computation of the phase-shift resulting from the only modification of the switches (UP/DOWN) state is instantaneous because it does not require the recalculation of the scale changing networks. Boundary conditions are artificially introduced in the formulation of the scale changing technique. These boundary conditions enclose the various scale-dependent domains and consequently, the derivation of the scale changing network reduces to the analysis of the cascade of planar discontinuity planes. For unbounded or non planar structures such approach requires additional approximations and consequently, is less attractive than in case of planar and bounded circuits.

III. COMPUTATIONAL RESULTS

The phase shifter shown in Fig. 1 has been characterized in Ku-band frequency range [10, 11] and the measurement technique is reported in [12]. The planar phase-shifter is located in the cross-section of a metallic square waveguide. Fig. 6 displays the elements of the measurement cell. The numerical and experimental data are reported in Fig. 7 for *4* various MEMS configurations (see figure caption of Fig. 7). A very good agreement is observed between results obtained from the scale changing technique and measurements in the whole frequency band. Fig. 8 displays the phase-shift variation versus the discrete (2^{10}=*1024*) accessible states of the *10* RF-MEMS switches. We observe a phase-shift range of about *360*° and the maximum phase-shift between two successive configurations is less than *10*°.

The proposed scale changing approach is much better than the Finite Element Method (FEM) software in time costing. Fig. 9 displays the computation time for calculating the phase-shift in a given MEMS switches configuration. Electromagnetic simulations are carried out on a PC with *1Giga* of RAM and *1.8GHz* clock frequency. The number of passive modes at the largest scale (Ω_0-domain) is tuned from *1000* to *4150* (with step of *50*). The number of modes in the intermediate $\Omega_k^{i,j}$ domains is chosen so that their number per m^2 is constant. For comparison purposes the number of tetrahedrons used in the FEM-based software is tuned form *1799* to *106.460* corresponding to *1* to *16* passes with 35% of mesh refinement per pass. The initial mesh in the FEM-based software is set so that most element lengths are approximately one-quarter wavelength. Fig. 9 indicates that the convergence is reached in *470s* by adopting *3350* active modes in the scale changing technique (with an error equals to *0.16*%) while *1300s* are required with the commercial software for obtaining a result with an error equals to *7.2*%. The CPU time for the calculation of the phase-shift is *2,5* times less than that of the FEM-based software. Moreover, the computation by the Scale Changing Technique of all the 1024 available phase-shifts is quasi-instantaneously. Now let us consider the computation of the phase-shift for the *1024* accessible RF-MEMS configurations. The admittance matrix obtained from the cascade of the *4* scale changing networks allows modelling the electromagnetic coupling between the largest scale $s_l=0$ and the smallest scale $s_l=4$. This matrix does not depend

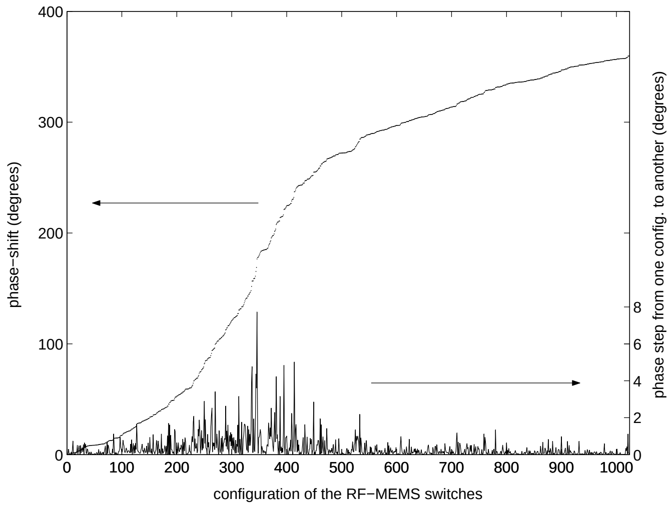

Fig. 8. Phase shift versus the configurations of the RF-MEMS switches (*1024* configurations are accessible with *10* RF-MEMS switches in UP or DOWN state) at 11.7GHz.

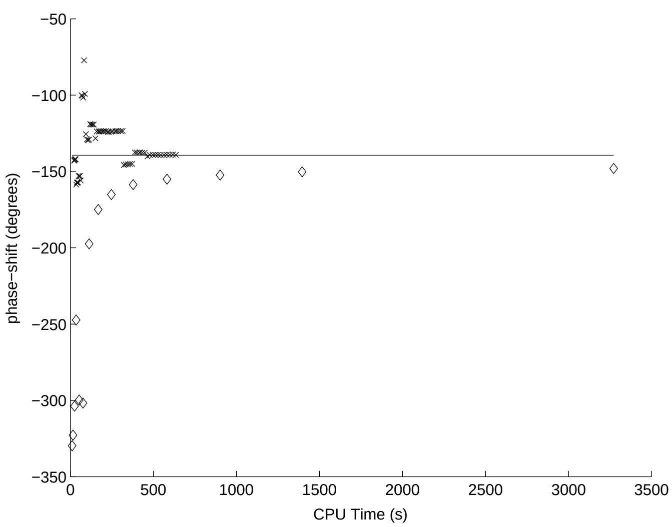

Fig. 9. Phase shift versus the computation time for the configuration A (see Fig. 7). Computation time varies with the number of tetrahedrons (in FEM-based software) or with the number of modes (in the scale changing technique). It is shown that the convergence of the computational results is reached more rapidly in the scale changing technique than in the FEM-based software. Moreover, when the convergence is reached, a very good agreement is obtained between results obtained from the scale changing technique and measurements. (—) Measurements; (×××) scaling changing technique and (◊◊◊) FEM-based software.

on the state of the MEMS switches and its size is *11x11*. The 2^{10} configurations associated with the UP/DOWN states of the *10* MEMS switches are modeled by *10* shunt impedances. Once the admittance matrix is calculated, only *10* seconds of computation time are required to sweep the *1024* possible configurations of the *10* switches. For technological reasons, the UP-state capacitance C_{up} of RF-MEMS switches is set to *15fF*. Let us find the DOWN-state capacitance C_{down} allowing a phase dynamics close to *360°*. This problem of great practical importance can not be solved easily by using FEM-based software due high time-consuming [10,11] but is efficiently solved by applying the Scale Changing Technique. Fig. 10

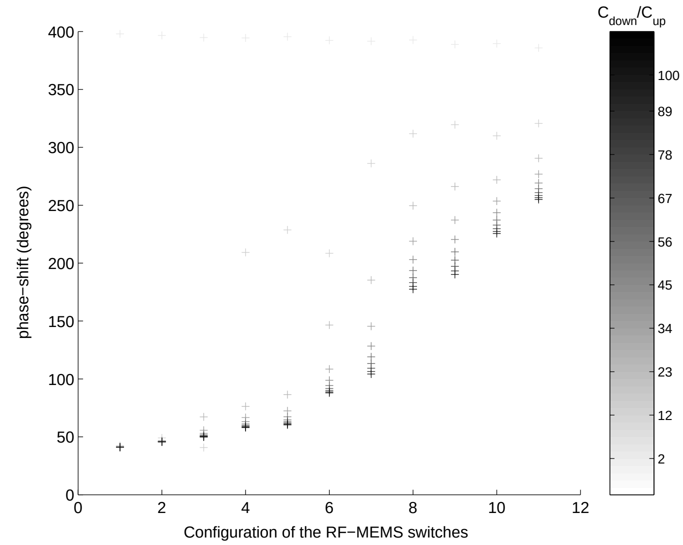

Fig. 10. Phase shift versus the configurations of the RF-MEMS switches for various ratios C_{down}/C_{up} (C_{up} = *15fF*) at *11.7GHz*.

represents the obtained variation of the phase-shift versus the RF-MEMS configurations for various ratios C_{down}/C_{up} and allows choosing easily the DOWN-state capacitance. For achieving a phase dynamics close to *360°* one may choose $C_{down}/C_{up} > 30$.

IV. CONCLUSION

A scale changing technique has been reported and applied with success to the electromagnetic modelling of MEMS-controlled planar phase-shifter. A very good agreement has been observed between computational results and measurements in the whole frequency band. Very good performances in terms of accuracy and CPU time have been obtained. The application of the sale changing technique for the electromagnetic modelling of reflectarrays composed of a finite number of MEMS-controlled planar phase-shifters is under way. The Scale Changing Technique is a generic approach and is not only applicable to RF MEMS-Based reflectarray antennas. It can be advantageously applied to microwave or millimeterwave circuits with high (pathological) aspect ratios and to planar multiscale (or fractal) structures.

APPENDIX

EXPRESSION OF $[Y_{0,1}]$ IN FIG. 5:

$$[Y_{0,1}] = \begin{bmatrix} Y_{0,1_{11}} & Y_{0,1_{12}} \\ Y_{0,1_{21}} & Y_{0,1_{22}} \end{bmatrix}$$

$$Y_{0,1_{11}} = Y^{(0)}_{M_a 1} + {}^tP_0 \left(P'_0 Z_0 \, {}^tP'_0\right)^{-1} P_0 \quad (4)$$

$$Y_{0,1_{12}} = -\, {}^tP_0 \left(P'_0 Z_0 \, {}^tP'_0\right)^{-1} \quad (5)$$

$$Y_{0,1_{21}} = -\left(P'_0 Z_0 \, {}^tP'_0\right)^{-1} P_0 \quad (6)$$

$$Y_{0,1_{22}} = \left(P'_0 Z_0 \, {}^tP'_0\right)^{-1} \quad (7)$$

where ${}^tP_0$ is the transpose of the matrix P_0. The element $(p_{0u,v})$ of the matrix P_0 where $u = (m, n, [TE, TM])$, $v =$

$(m',n',[TE,TM])$, $(m,n)\in[1:N_{0_m}]$x$[1:N_{0_n}]$, $(m',n')\in[1:N_{1_m}]$x$[1:N_{1_n}]$ is given by

$$(p_{0u,v})=\left\langle \mathbf{f}_{_{0u}},\mathbf{f}_{_{1v}}\right\rangle$$

$\mathbf{f}_{_{iu}}$ $(i=[0,1])$ denotes the TE and TM modes in the Ω_i domain and $\langle\ ,\ \rangle$ is the inner product. The element $\left(p'_{0u,v}\right)$ of P'_0 has the same expression as $(p_{0u,v})$ but with $(m,n)\in[N_{0_m}+1:M_{0_m}]x[N_{0_n}+1:M_{0_n}]$.

The element $(z_{0u,u})$, $u=(m,n,[TE,TM])$, $(m,n)\in[N_{0_m}+1:M_{0_m}]x[N_{0_n}+1:M_{0_n}]$ of Z_0 is given by

$$z_{0u,u}=Z^{(a)}_{M0(u,u)}-\frac{\left(Z^{(a)}_{M0(u,u)}\right)^2}{Z^{(a)}_{M0(u,u)}+Z^{(b)}_{M0(u,u)}}$$

where the indices a and b refer to the notations of Fig. 2, and $p=[a,b]$:

$$Z^p_{M0(u,u)}=\begin{cases} Z^p_{M0(m,n,TE)}=\frac{\gamma^p_{0(m,n)}}{j\omega\mu_0}\\ Z^p_{M0(m,n,TM)}=\frac{j\omega\varepsilon_0\varepsilon^{(p)}_r}{\gamma^p_{0(m,n)}}\end{cases}$$

where $\gamma^p_{0(m,n)}$ represents the complex propagation constant of the guided modes on the waveguide of cross section Ω_0 (see Fig. 2). Y^a_{M01} in relation (4) is given by $Y^a_{M01}=Y^a_{M0(1,0,TE)}=\frac{1}{Z^a_{M0(1,0,TE)}}$.

EXPRESSION OF $[Z_{1,2}]$ IN FIG. 5:

$$[Z_{1,2}]=\begin{bmatrix} P_1\left({}^tP'_1Y_{M_1}P'_1\right)^{-1}\ {}^tP_1 & -P_1\left({}^tP'_1Y_{M_1}P'_1\right)^{-1}\\ -\left({}^tP'_1Y_{M_1}P'_1\right)^{-1}\ {}^tP_1 & \left({}^tP'_1Y_{M_1}P'_1\right)^{-1}\end{bmatrix}$$

where $P_1={}^t\left[P^{(1)}_1\ P^{(2)}_1\right]$. The element $\left(p^{(i)}_{1u,v}\right)$ of $P^{(i)}_1$ $(i=[1,2])$ where $u=(m,n,[TE,TM])$, $v=(m',n',[TE,TM])$, $(m,n)\in[1:N_{1_m}]$x$[1:N_{1_n}]$, $(m',n')\in\left[1:N^i_{2_m}\right]x\left[1:N^i_{2_n}\right]$, $(TE\ m\neq0,TM\ n\neq0)$ is given by

$$\left(p^{(i)}_{1u,v}\right)=\left\langle \mathbf{f}_{_{1u}},\mathbf{f}^{(i)}_{_{2v}}\right\rangle$$

$\mathbf{f}^{(i)}_{_{2v}}$ $(i=[1,2])$ denotes the TE and TM modes in the Ω^i_2 domain. $P'_1={}^t\left[P'^{(1)}_1\ P'^{(2)}_1\right]$ and the element $\left(p'^{(i)}_{1u,v}\right)$ of $P'^{(i)}_1$, $(i=[1,2])$ has the same expression as $\left(p^{(i)}_{1u,v}\right)$ but with $(m,n)\in[N_{1_m}+1:M_{1_m}]x[N_{1_n}+1:M_{1_n}]$.

The element $\left(Y_{M1(u,u)}\right)$, $u=(m,n,[TE,TM])$, $(m,n)\in[N_{1_m}+1:M_{1_m}]x[N_{1_n}+1:M_{1_n}]$ of Y_{M_1} is given by

$$Y_{M_1(u,u)}=\begin{cases} Y_{M_1(m,n,TE)}=\frac{\gamma^a_{1(m,n)}}{j\omega\mu_0}+\frac{\gamma^b_{1(m,n)}}{j\omega\mu_0}\\ Y_{M_1(m,n,TM)}=\frac{j\omega\varepsilon_0\varepsilon^{(a)}_r}{\gamma^a_{1(m,n)}}+\frac{j\omega\varepsilon_0\varepsilon^{(b)}_r}{\gamma^b_{1(m,n)}}\end{cases}$$

where $\gamma^p_{1(m,n)}$ $(p=[a,b])$ is related to Ω_1.

EXPRESSION OF $\left[Y^i_{2,3}\right]$, $i=[1,2]$ IN FIG. 5:

$$\begin{aligned}
\left[Y^i_{2,3}\right] &= \begin{bmatrix} Y^i_{2,3_{11}} & Y^i_{2,3_{12}}\\ Y^i_{2,3_{21}} & Y^i_{2,3_{22}}\end{bmatrix}\\
Y^i_{2,3_{11}} &= -P^{(i)}_2\left({}^tP'^{(i)}_2Z^{(i)}_{M_2}P'^{(i)}_2\right)^{-1}\\
Y^i_{2,3_{12}} &= P^{(i)}_2\left({}^tP'^{(i)}_2Z^{(i)}_{M_2}P'^{(i)}_2\right)^{-1}\ {}^tP^{(i)}_2\\
Y^i_{2,3_{21}} &= \left({}^tP'^{(i)}_2Z^{(i)}_{M_2}P'^{(i)}_2\right)^{-1}\\
Y^i_{2,3_{22}} &= -\left({}^tP'^{(i)}_2Z^{(i)}_{M_2}P'^{(i)}_2\right)^{-1}\ {}^tP^{(i)}_2
\end{aligned}$$

where $P^{(i)}_2={}^t\left[P^{(i,1)}_2\ P^{(i,2)}_2\ P^{(i,3)}_2\ P^{(i,4)}_2\ P^{(i,5)}_2\right]$. The element $\left(p^{(i,j)}_{2u,v}\right)$ of $P^{(i,j)}_2$, $(i=[1,2]\,,\ j=[1:5])$ where $u=(m,n,[TE,TM])\,,\ v=(m',n',[TE,TM])$, $(m,n)\in\left[1:N^i_{2_m}\right]x\left[1:N^i_{2_n}\right]$, $(m',n')\in\left[1:N^{i,j}_{3_m}\right]x\left[1:N^{i,j}_{3_n}\right]$, $(TE\ m\neq0,TM\ n\neq0)$, $(TE\ m'\neq0,TM\ n'\neq0)$ is given by

$$\left(p^{(i,j)}_{2u,v}\right)=\left\langle \mathbf{f}^{(i)}_{_{2u}},\mathbf{f}^{(i,j)}_{_{3v}}\right\rangle$$

$\mathbf{f}^{(i,j)}_{_{3v}}$ $(i=[1,2]\,,\ j=[1:5])$ denotes the TE and TM modes in the $\Omega^{i,j}_3$ domain. $P'^{(i)}_2={}^t\left[P'^{(i,1)}_2\ P'^{(i,2)}_2\ P'^{(i,3)}_2\ P'^{(i,4)}_2\ P'^{(i,5)}_2\right]$ and the element $\left(p'^{(i,j)}_{2u,v}\right)$ of $P'^{(i,j)}_2$, $i=[1,2]$, $j=[1:5]$, has the same expression as $\left(P^{(i,j)}_2\right)$ but with $(m,n)\in[N_{1_m}+1:M_{1_m}]x[N_{1_n}+1:M_{1_n}]$.

The element $\left(Z^{(i)}_{M2(u,u)}\right)$, $i=[1,2]$, $u=(m,n,[TE,TM])$, $(m,n)\in\left[N^i_{2_m}+1:M^i_{2_m}\right]x\left[N^i_{2_n}+1:M^i_{2_n}\right]$ of $Z^{(i)}_{M_2}$ is given by

$$Z^{(i)}_{M2(u,u)}=\begin{cases} Z^{(i)}_{M2(m,n,TE)}=\dfrac{\frac{j\omega\mu_0}{\gamma^{(1)}_{a(m,n)}}*\frac{j\omega\mu_0}{\gamma^{(1)}_{b(m,n)}}}{\frac{j\omega\mu_0}{\gamma^{(1)}_{a(m,n)}}+\frac{j\omega\mu_0}{\gamma^{(1)}_{b(m,n)}}},\\ Z^{(i)}_{M2(m,n,TM)}=\dfrac{\frac{\gamma^{(1)}_{a(m,n)}}{j\omega\varepsilon_0\varepsilon^{(a)}_r}*\frac{\gamma^{(1)}_{b(m,n)}}{j\omega\varepsilon_0\varepsilon^{(b)}_r}}{\frac{\gamma^{(1)}_{a(m,n)}}{j\omega\varepsilon_0\varepsilon^{(a)}_r}+\frac{\gamma^{(1)}_{b(m,n)}}{j\omega\varepsilon_0\varepsilon^{(b)}_r}}\end{cases}$$

where $\gamma^{p(i)}_{2(m,n)}$ $(p=[a,b])$ is related to $\Omega^{(i)}_2$.

EXPRESSION OF $\left[Z^{(i,j)}_{3,4}\right]$, $i=[1,2]\,,\ j=[1:5]$ IN FIG. 5:

$$\begin{aligned}
\left[Z^{(i,j)}_{3,4}\right] &= \begin{bmatrix} Z^{(i,j)}_{3,4_{11}} & Z^{(i,j)}_{3,4_{12}}\\ Z^{(i,j)}_{3,4_{21}} & Z^{(i,j)}_{3,4_{22}}\end{bmatrix}\\
Z^{(i,j)}_{3,4_{11}} &= P^{(i,j)}_3\left({}^tP'^{(i,j)}_3Y^{(i,j)}_{M_3}P'^{(i,j)}_3\right)^{-1}\ {}^tP^{(i,j)}_3\\
Z^{(i,j)}_{3,4_{12}} &= -P^{(i,j)}_3\left({}^tP'^{(i,j)}_3Y^{(i,j)}_{M_3}P'^{(i,j)}_3\right)^{-1}\\
Z^{(i,j)}_{3,4_{21}} &= -\left({}^tP'^{(i,j)}_3Y^{(i,j)}_{M_3}P'^{(i,j)}_3\right)^{-1}\ {}^tP^{(i,j)}_3\\
Z^{(i,j)}_{3,4_{22}} &= \left({}^tP'^{(i,j)}_3Y^{(i,j)}_{M_3}P'^{(i,j)}_3\right)^{-1}
\end{aligned}$$

The element $\left(p_{3u,v}^{(i,j)}\right)$ of $P_3^{(i,j)}$, $i=[1,2]$, $j=[1:5]$ where $u=(m,n,[TE,TM])$, $v=(m',n',[TE,TM])$, $(m,n)\in\left[1:N_{3_m}^{i,j}\right]\text{x}\left[1:N_{3_n}^{i,j}\right]$, $(m',n')\in\left[1:N_{4_m}^{i,j}\right]\text{x}\left[1:N_{4_n}^{i,j}\right]$, $(TE\ m\neq 0, TM\ n\neq 0)$, $(TE\ m'\neq 0, TM\ n'\neq 0)$ is given by

$$\left(p_{3u,v}^{(i,j)}\right)=\left\langle \mathbf{f}_{_{3^u}}^{(i,j)},\mathbf{f}_{_{4^v}}^{(i,j)}\right\rangle$$

$\mathbf{f}_{_{4^v}}^{(i,j)}$ $(i=[1,2]\,,\,j=[1:5])$ denotes the TE and TM modes in the $\Omega_4^{i,j}$ domain. The element $\left(p_{3u,v}^{\prime(i,j)}\right)$ of $P_3^{\prime(i,j)}$, $i=[1,2]$, $j=[1:5]$, has the same expression as $\left(P_3^{(i,j)}\right)$ but with $(m,n)\in\left[N_{3_m}^{i,j}+1:M_{3_m}^{i,j}\right]\text{x}\left[N_{3_n}^{i,j}+1:M_{3_n}^{i,j}\right]$.

The element $\left(Y_{M_3(u,u)}^{(i,j)}\right)$, $i=[1,2]$, $j=[1:5]$, $u=(m,n,[TE,TM])$, $(m,n)\in\left[N_{3_m}^{i,j}+1:M_{3_m}^{i,j}\right]\text{x}\left[N_{3_n}^{i,j}+1:M_{3_n}^{i,j}\right]$ of $Y_{M_3}^{(i,j)}$ is given by

$$Y_{M_3(u,u)}^{(i,j)}=\left\{\begin{array}{l} Y_{M_3(m,n,TE)}^{(i,j)}=\frac{\gamma_{3(m,n)}^{a(i,j)}}{j\omega\mu_0}+\frac{\gamma_{3(m,n)}^{b(i,j)}}{j\omega\mu_0} \\ Y_{M_3(m,n,TM)}^{(i,j)}=\frac{j\omega\varepsilon_0\varepsilon_r^{(a)}}{\gamma_{3(m,n)}^{a(i,j)}}+\frac{j\omega\varepsilon_0\varepsilon_r^{(b)}}{\gamma_{3(m,n)}^{a(i,j)}} \end{array}\right.$$

where $\gamma_{3(m,n)}^{p(i,j)}$ $(p=[a,b])$ is related to $\Omega_3^{(i,j)}$.

ACKNOWLEDGMENT

The authors wish to thank Dr. Etienne GIRARD for providing the measurements of the planar phase-shifter.

REFERENCES

[1] D. G. Berry, R. G. Malech and W. A. Kennedy, ”The Reflectarray Antenna,” *IEEE Trans. Antennas Propagat.*, Vol. 11, pp. 645-651, Nov. 1963.

[2] K. Y. Sze, L. Shafai, ”Phase properties of single-layer patch arrays with applications to line-source-fed microstrip reflectarrays,” *IEEE Proc. Microwave Antennas Propagat.*, Vol. 149, Issue 1, pp. 64-70, Feb. 2002.

[3] J. Huang, ”Microstrip reflectarray,” *Antennas and Propagation Society International Symposium*, AP-S. Digest, pp. 612-615, 1991.

[4] J. Huang, ”Analysis of a Microstrip Reflectarray Antenna for Microspacecraft Applications,” *JPL TDA Progress Report*, No.42-120, pp. 153-172, Feb. 1995.

[5] R.D. Javor, Xiao-Dong Wu, and Kai Chang, ”Design and performance of a microstrip reflectarray antenna,” *Microwave and Optical Technology Letters*, Vol. 7, No. 7, pp. 322-324, May 1994.

[6] S. D. Targonski, D.M. Pozar, ”Analysis and design of a microstrip reflectarray using patches of variable size,” *Antennas and Propagation Society International Symposium*, Vol. 3, pp. 1820 – 1823, 20-24 June 1994.

[7] J. Encinar, L. Datashvili, H. Baier, M. Arrebola, M. Sierra-Castaner, J.L. Besada, H. Legay, G. Toso, ”*Breadboard of a three layer printed reflectarray for dual polarization and dual coverage*,” 28th ESA Antenna Technology Workshop on Space Antenna Systems and Technologies, Noordwijk, pp. 443-448, 20-31 May 2005.

[8] J. P. Gianvittorio, Y. Rahmat-Samii, ”Reconfigurable reflectarray with variable height patch elements: design and fabrication,” *Antennas and Propagation Society Symposium*, Vol. 2, pp. 1800 – 1803, 20-25 June 2004.

[9] H. Legay, B.Pinte, M. Charrier, A. Ziaei, E. Girard, R. Gillard, ”A steerable reflectarray antenna with MEMS controls,” *IEEE International Symposium on Phased Array Systems and Technology*, pp. 494–499, 14-17 Oct. 2003.

[10] H. Legay, G. Caille, P. Pons, E. Perret, H. Aubert, J. Pollizzi, A. Laisne, R. Gillard, M. Van Der Worst, ”MEMS Controlled Phase-Shift Elements for a Linear Polarised Reflectarray,” 28^th *ESA Antenna Technology Workshop on Space Antenna Systems and Technologies*, Noordwijk, pp. 443-448, 20-31 May 2005.

[11] H. Legay et al., ”MEMS technology for Terminals and Satellite Antennas,” *ESTEC Final Report*, Contract N 17269/03/NL/AG, September 2005.

[12] D. Cadoret, A. Laisne, R. Gillard, H. Legay, ”New reflectarray cell using coupled microstrip patches loaded with slots”, *Microwave and Optical Technical Letters*, February 2005, , vol. 44, No. 3, pp. 270-273.

[13] M. Nadarassin, H. Aubert, and H. Baudrand, ”Analysis of planar structures by an integral approach using entire domain trial functions,” *IEEE Transactions on Microwave Theory Techniques*, Volume 43, number 10, pp. 2492 – 2495, October 1995.

[14] E. Perret, H. Aubert, ”Scale changing technique for the computation of the input impedance of active patch antennas,” *IEEE Antennas and Wireless Propagation Letters*, Vol. 4, 2005 Pages: 326 - 328.

[15] E. Perret, H. Aubert, and R. Plana, ”N-Port Network for the electromagnetic modeling of MEMS switches,” *Microwave and Optical Technology Letters*, 5 April 2005, Vol. 45, No. 1, pp. 46 – 49.

[16] J.W. Tao, H.Baudrand, ”Multimodal variational analysis of uniaxial waveguide discontinuities,” *IEEE Trans. on Microwave Theory and Techniques*, Vol. 39, Issue 3, pp. 506 – 516, March 1991.